AGU PUBLICATIONS

JGR

Journal of Geophysical Research: Solid Earth

RESEARCH ARTICLE

10.1002/2017JB014176

Frequency dependence of susceptibility in magnets with uniaxial and triaxial anisotropy

A. J. Newell[1]

[1] Department of Marine, Earth, and Atmospheric Sciences, North Carolina State University, Raleigh, North Carolina, USA

Key Points:
- Theory of frequency dependence of magnetic susceptibility in arbitrarily oriented magnetic minerals
- Response has a sharp peak near the superparamagnetic/single-domain critical size
- The anisotropy can be used to determine the strain in a rock and correct paleofield directions

Supporting Information:
- Supporting Information S1
- Data Set S1
- Data Set S2
- Data Set S3
- Data Set S4

Correspondence to:
A. J. Newell,
Andrew_Newell@ncsu.edu

Citation:
Newell, A. J. (2017), Frequency dependence of susceptibility in magnets with uniaxial and triaxial anisotropy, *J. Geophys. Res. Solid Earth*, *122*, 7544–7561, doi:10.1002/2017JB014176.

Received 8 MAR 2017
Accepted 18 JUL 2017
Accepted article online 20 JUL 2017
Published online 30 OCT 2017

Abstract Characterization of minerals in rocks and soils provides a window into environmental processes and improves the interpretation of paleomagnetic measurements. Mineral composition, size, and shape can be constrained using magnetic measurements. For small minerals, a promising measurement is the frequency dependence of magnetic susceptibility. The size and shape dependence of the in-phase component $\chi'(\omega)$ and out-of-phase component $\chi''(\omega)$ are derived for arbitrarily oriented superparamagnetic and single-domain magnets with uniaxial and triaxial anisotropy. In a fluctuating field, a single magnet has a thermal response parallel to the easy axis and instantaneous rotation of the moment perpendicular to it. The size and temperature variations have the same form as in earlier theories in which all the magnets are aligned with the field and can be easily adapted to the methods of Shcherbakov and Fabian (2005) and Egli (2009) for finding size distributions using multiple temperatures and frequencies. These inversions are inherently nonunique and complicated by non-SD contributions, but some robust constraints can be put on the volume distribution if the commonly used ratio χ_{fd} is 10% or greater. The anisotropy of the out-of-phase component (opAMS) has the same sense as thermoremanent magnetization (TRM) and can be used to correct the paleofield direction. Along with the anisotropy of the in-phase component (ipAMS), it can be used to gain quantitative information on the deformation of the host rock. For the line/plane, or March, deformation model, opAMS and ipAMS are calculated and it is shown how they can be used to accurately represent the strain anisotropy.

Plain Language Summary Magnetic measurements can be a quick, noninvasive tool to gain information on minerals in rocks and soils, providing insight into past environmental conditions. It has been difficult to quantify this information because the sources are complex. A particularly useful method may be to apply small oscillating fields and measure the response. In this article, a comprehensive theory is presented for this method in very small magnetic minerals. Previous theories, which were for magnets aligned with the magnetic field, have been extended to random orientations. This can be used with previous inversion tools to get better estimates of size distributions, and it opens up new possibilities for analyzing the anisotropy of the signal. In particular, the anisotropy is derived for a widely used model of tectonic deformation, and it can be used to get an accurate estimate of the deformation. The anisotropy can also be used to correct the direction of ancient fields in paleointensity measurements.

1. Introduction

1.1. Particle Size Distributions

Superparamagnetic (SP) and single-domain (SD) magnets have sizes of tens of nanometers or less and include the most reliable recorders of the Earth's magnetic field. They are also important parts of environmental processes such as the iron cycle, soil formation, diagenesis [*Schwartz et al.*, 1997; *Tarduno*, 1995] and magnetoreception [*Kirschvink and Walker*, 1985]. As a result, they can provide useful information on paleoclimate, pollution and other environmental processes [*Thompson and Oldfield*, 1986; *Evans and Heller*, 2003; *Liu et al.*, 2012] Magnetic measurements can be used to constrain properties such as composition, grain size and shape.

Traditionally, ratios of hysteresis parameters have been used to indicate grain size. Examples include ARM/SIRM and SIRM/χ, where ARM is anhysteretic remanent magnetization, SIRM is saturation isothermal remanent magnetization (often denoted by M_{rs}), and χ is the volumetric low-field susceptibility. Plots of ratios against each other are also used, particularly the Day plot (H_{cr}/H_c versus M_{rs}/M_s, where H_c is the coercivity, H_{cr} the coercivity of remanence, and M_s the saturation magnetization) and the King plot (χ_{ARM} versus χ, where χ_{ARM} is the anhysteretic remanent susceptibility) [*Evans and Heller*, 2003, pp. 21–24].

In principle, more information can be obtained from detailed coercivity spectra, in which an isothermal remanent magnetization (IRM) is progressively demagnetized in an alternating field (AF) or DC field [*Dunlop*, 1986; *Robertson and France*, 1994; *Egli*, 2004a, 2004b]. Even more data are provided by first-order reversal curve (FORC) analysis, which is based on the Preisach model of hysteresis [*Mayergoyz*, 1991; *Pike et al.*, 1999]. One feature of a FORC diagram that is particularly diagnostic of uniaxial, noninteracting SD magnets is a narrow ridge along the H_c axis [*Newell*, 2005; *Egli et al.*, 2010]. However, since a FORC diagram extracts the hysteresis from magnetization curves, it cannot represent a signal from SP magnets.

Another approach that is useful for analyzing SP particles is progressive thermal demagnetization of a remanence, which can be analyzed using the classic *Néel* [1949] theory. *Worm and Jackson* [1988] used this to determine the size distribution of small titanomagnetite grains in Yucca Mountain Tuff. This required the assumption that the distribution of particle shapes (or other sources of anisotropy) is much narrower than the distribution of volumes [*Jackson et al.*, 2006].

In an attempt to determine a joint distribution for volumes and anisotropies, *Dunlop* [1965] developed thermal fluctuation analysis, which involves AF demagnetization of partial thermoremanent magnetizations (pTRMs) acquired over a series of temperature intervals. The idea behind this is that in single-domain magnets, the coercivity of remanence is determined by a combination of anisotropy and thermal fluctuations, and the two effects are approximately additive. For low temperatures, *Jackson et al.* [2006] substituted DC demagnetization for AF demagnetization and called it thermal fluctuation tomography.

A single-domain magnet has a simple hysteresis loop consisting of two branches. The field at which the magnetization jumps from the lower branch to the upper is known as the switching field and coincides with the coercivity of remanence. It depends on the relative orientation of the magnet and the magnetic field in a nonlinear way, as does the size of the jump [*Stoner and Wohlfarth*, 1948; *Newell*, 2000, Figure 2]. When the magnet becomes large enough for nonuniform reversals to occur, new states become available for jumps and there are generally multiple jumps [*Newell and Merrill*, 2000]. The single-domain size range increases as the magnets become more elongated, but this increase is much more gradual for the reversal mode than for remanence. In magnetite, the upper size for uniform reversal rises from 55 nm to 89 nm (cube root of volume) as the aspect ratio goes from 1 to 10 (equation (81)).

In an SD magnet, the coercivity of remanence decreases with decreasing size because of more frequent barrier hopping due to thermal fluctuations. In larger magnets, it decreases with increasing size as nonuniform reversal modes become available. These two effects cannot be distinguished in an analysis of coercivity spectra. There is little systematic knowledge of how hysteresis parameters vary with size, shape, and other factors in larger magnets.

Another measurement that has been used to estimate size distributions of single-domain magnets is the frequency dependence of magnetic susceptibility $\chi(\omega)$. In small magnets, this has a phase shift compared to the applied field, and it is generally separated into an in-phase component χ' and an out-of-phase, or quadrature, component χ''. Both have a strong size dependence with a narrow peak near the boundary between SP and SD behavior. A common procedure is to measure a susceptibility χ'_{lf} at a relatively low frequency (usually 470 Hz) and another, χ'_{hf}, at a higher frequency (4.7 kHz). The ratio

$$\chi_{\mathrm{fd}} = \frac{\chi'_{\mathrm{lf}} - \chi'_{\mathrm{hf}}}{\chi'_{\mathrm{lf}}}, \tag{1}$$

expressed as a percentage, is used to represent the frequency dependence [*Thompson and Oldfield*, 1986].

Large values of χ_{fd} are seen in paleosol layers [*Evans and Heller*, 2003, pp. 71]. For many samples the maximum value of χ_{fd} is about 15% [*Worm*, 1998], although *Worm and Jackson* [1999] obtained a maximum of 30% in Yucca Mountain Tuff. By contrast, in coarse MD magnetite it is at most 0.3% [*Thompson and Oldfield*, 1986]. The first attempts to explain the maximum value using expressions for the zero-frequency susceptibility [*Dearing et al.*, 1996; *Eyre*, 1997] were already out of date, since *Néel* [1949] had derived an expression for the in-phase component of frequency-dependent susceptibility in SP magnets and *Mullins and Tite* [1973] had extended it to the quadrature component.

A single parameter can only provide limited information on the size distribution. *Liu et al.* [2005] used measurements at two frequencies (1 Hz and 10 Hz) over temperatures from 10 K to 300 K to determine a more

detailed size distribution. *Shcherbakov and Fabian* [2005] modeled multiple frequencies at a range of temperatures. They noted that other factors, particularly particle shape, complicate the inversion because they affect hysteresis properties and energy barriers. For a joint distribution of energy barriers and volumes, they found a dispersion relation between χ' and χ'' that generalizes that of *Néel* [1949]. This dispersion relation makes the two measurements redundant, reducing the amount of information available for inversion. *Shcherbakov and Fabian* [2005] showed how various assumptions about the energy barrier distribution could be incorporated in an inversion for the volume distribution. They also added a mean field approximation for the effect of particle interactions.

Egli [2009] pointed out that the Stoner-Wohlfarth model may not accurately describe SP and SD magnets because of a variety of surface effects that can be difficult to quantify. He adapted a more general phenomenological model by Shliomis, Stepanov, and Raikher [*García-Palacios*, 2000] to the methods of *Shcherbakov and Fabian* [2005], including the effect of particle interactions.

1.2. Anisotropy

All the above models are for a geometry in which the easy axes of all the magnets are parallel to the magnetic field. In general, they are randomly oriented, although there may be preferred directions. At the zero-frequency limit, anisotropy of magnetic susceptibility (AMS) is a widely used tool in environmental and tectonic studies, providing information on processes such as deformation in rocks and paleocurrents [*Tarling and Hrouda*, 1993; *Evans and Heller*, 2003]. However, AMS includes contributions from paramagnetic and diamagnetic minerals as well as ferrimagnetic minerals. It can be advantageous to separate these subfabrics, and methods have been developed for this purpose [*Martín-Hernández and Ferré*, 2007]. The anisotropy of the out-of-phase (quadrature) component, or opAMS, has no contribution from diamagnetic or paramagnetic sources. Minerals such as pyrrhotite, titanomagnetites, and hematite have a nonzero quadrature component because of low-field hysteresis, while SP and SD magnetite and maghemite particles also contribute [*Hrouda et al.*, 2017].

SD magnets have a direction of maximum susceptibility that is perpendicular to the direction of maximum remanence, resulting in an "inverse fabric" [*Rochette*, 1988; *Borradaile and Puumala*, 1989; *Potter and Stephenson*, 1988]. While this is not common, it can reduce the apparent normal fabric in volcanic rocks [*Hrouda and Jeżek*, 2017].

Anisotropy of susceptibility or remanence can be used to correct the directions of natural remanent magnetization (NRM) for deformation or other sources of anisotropy. For this purpose, AMS is not generally used because of the inverse fabric. Instead, TRM has been corrected using anisotropy of isothermal remanent magnetization (IRM) [*Janák*, 1967; *Stephenson et al.*, 1986], anhysteretic remanent magnetization (ARM) [*McCabe et al.*, 1985], gyroremanent magnetization (GRM) [*Potter and Stephenson*, 1988] and lab-induced TRM [*Selkin et al.*, 2000].

Frequency-dependent susceptibility overcomes some of these problems. The ratio χ_{fd} enhances the contribution of SD magnets compared to paramagnetic or diamagnetic minerals as well as multidomain ferromagnets. Recent theoretical results also suggest that it can have a "normal fabric," which makes it a possible tool for correcting NRM directions.

To apply his theory of frequency-dependent susceptibility to collections of randomly oriented magnets, *Néel* [1949] represented them by a model collection in which two thirds have easy axes perpendicular to the field, contributing nothing to the response, while the other third have axes parallel to the field. *Lanci and Zanella* [2016] claimed to have explicitly calculated the frequency dependence of susceptibility for any angle between the magnetic field and the easy axis. They used it to calculate the AMS as a function of frequency, finding that the maximum susceptibility of an SP magnet is parallel to the easy axis, in contrast to SD magnets where it is perpendicular. However, I will show that their derivation was based on an incorrect assumption.

The goals of this article are (1) to obtain a correct derivation of the frequency dependence of susceptibility for SD magnets with uniaxial and triaxial anisotropy; (2) to determine how the intrinsic anisotropy of the magnets combines with the anisotropy of easy axis orientations to determine ipAMS and opAMS, the anisotropies of the in-phase and quadrature components; and (3) to calculate how the susceptibility is modified when there is a volume distribution. These are preliminary steps toward a more rigorous interpretation of frequency-dependent susceptibility in natural samples.

1.3. The Néel Theory

In Néel's theory [*Néel*, 1949; *Mullins and Tite*, 1973; *Shcherbakov and Fabian*, 2005], there are two stable states that vary with the magnetic field, resulting in the two branches of the hysteresis loop. Let the fraction of states with magnetization in the positive direction be $n_+(t)$ and the fraction in the opposite direction be $n_-(t)$, with

$$n_+(t) + n_-(t) = 1. \tag{2}$$

If $\nu_+(t)$ is the frequency of transitions from the + to the − state and $\nu_-(t)$ is the rate in the reverse direction, the time dependence of the probabilities satisfies the pair of differential equations

$$\dot{n}_+ = -\dot{n}_- = \nu_- n_- - \nu_+ n_+. \tag{3}$$

The magnetization in the direction of the field is

$$M = n_+ M_+ + n_- M_-, \tag{4}$$

where all of the terms on the right depend on time through variations in the magnetic field. If the field is parallel to the easy axis, $M_\pm = \pm M_s$, where M_s is the saturation magnetization. Then equation (3) can be rearranged (using equation (2)) to get

$$\dot{n}_+ - \dot{n}_- = \nu_- - \nu_+ - \left(\nu_- + \nu_+\right)\left(n_+ - n_-\right). \tag{5}$$

Equivalently,

$$\dot{M} = \frac{1}{\tau}\left(M_{eq} - M\right), \tag{6}$$

where

$$\frac{1}{\tau} = \nu_+ + \nu_- \tag{7}$$

and

$$M_{eq} = M_s \frac{\nu_- - \nu_+}{\nu_- + \nu_+} \tag{8}$$

is the equilibrium magnetization that would be obtained if $\nu_\pm$ were held at their instantaneous values. In a small field H,

$$M_{eq} \approx \chi_0 H, \tag{9}$$

χ_0 being the static initial susceptibility for a superparamagnetic particle.

Now we suppose that a time-dependent field,

$$H = H_0 \exp(i\omega t), \tag{10}$$

is applied and the resulting magnetization has the form $M(t) = \chi(\omega)H(t)$. Then

$$\chi(\omega) = \frac{\chi_0}{1 + i\omega\tau}. \tag{11}$$

To find χ_0, we must solve the *Stoner and Wohlfarth* [1948] model to get the magnetization and the resulting energy barriers. In this model, each magnet has uniaxial anisotropy with a single easy axis. If θ is the acute angle between the field and the easy axis and ϕ is the angle between the positive field direction and the magnetization, the energy is (in SI units)

$$E = K_u V \sin^2(\phi - \theta) - \mu_0 M_s H V \cos\phi, \tag{12}$$

where V is the volume, M_s the saturation magnetization, μ_0 the permeability of free space, and K_u the uniaxial anisotropy parameter. Equilibrium solutions for a given θ and H satisfy

$$\frac{\partial E}{\partial \phi} = 2K_u V \sin(\phi - \theta)\cos(\phi - \theta) + \mu_0 M_s H V \sin\phi = 0. \tag{13}$$

When the field is parallel to the easy axis ($\theta = 0$), the solutions for small magnetic fields are $\phi = 0$ and $\phi = \pi$ (the energy minima with populations n_+ and n_-) and $\phi = \cos^{-1}\left(-\mu_0 M_s H/2K_u\right)$ (the energy maximum). The difference between the energy maximum E_{max} and the energy minima ($E_\pm$) determines the height of the energy barriers between stable states. The relaxation rates are

$$\nu_\pm = \nu_{th} \exp\left(-\frac{E_{max} - E_\pm}{k_B T}\right), \tag{14}$$

where ν_{th} is a prefactor of order 10^9 Hz, T is the temperature in kelvins, and k_B is Boltzmann's constant. These energies are

$$E_{max} = K_u V + \left(\frac{\mu_0 M_s H}{2K_u}\right)^2 V \tag{15a}$$

$$E_\pm = \mp \mu_0 M_s H V. \tag{15b}$$

To first order,

$$\nu_\pm = \exp\left(-\frac{K_u V}{k_B T}\right)\left(1 \mp \frac{\mu_0 M_s H V}{k_B T}\right). \tag{16}$$

Inserting this in equations (8) and (9) gives

$$\chi_0 = \frac{\mu_0 M_s^2 V}{k_B T}. \tag{17}$$

An essential step in the derivation of this standard result is the linear approximation for $\nu_\pm(H)$ when H is small.

Lanci and Zanella [2016] claimed to extend the theory to arbitrary field directions using a result from *McNamara and Wiesenfeld* [1989]. However, the result relies on the assumption that the relaxation rates have the form

$$\nu_\pm(t) = f(\mu \pm \eta_0 \cos\omega t). \tag{18}$$

Lanci and Zanella identify $f(t)$ as a multiple of an exponential (as in equation (14)), μ with $-K_u V/k_B T$ and η_0 with $-\mu_0 M_s H_0 V/k_B T$ (with $H = H_0 \cos\omega t$). Even for $\theta = 0$, the relaxation rate only has this form if the quadratic term in equation (15a) is ignored. Fortunately, the assumption is not necessary: *McNamara and Wiesenfeld* [1989] only used it to obtain a Taylor expansion for $\nu_\pm$ in the small parameter $\eta = \eta_0 \cos\omega t$, which they inserted in an integral solution of the rate equations (equation (3)). This is equivalent to the linearization of the rate equations in H by Néel.

When $\theta \neq 0$, the solutions of equation (13) are nonlinear implicit functions of H. Below, I will obtain Taylor expansions of the relaxation rates using implicit differentiation, and then I will solve the linearized rate equations directly; the integral solution by *McNamara and Wiesenfeld* [1989] is not needed. Surprisingly, this procedure is more straightforward in the more general case of triaxial anisotropy, so I will solve that first and then show how it must be modified to obtain the expansion for Stoner-Wohlfarth particles.

2. Triaxial Anisotropy

We suppose that a single-domain magnet has a triaxial anisotropy whose magnitude and direction are determined by a tensor **K**. In general, this is the sum of a magnetocrystalline anisotropy, inverse magnetostriction due to an external stress, and the shape of the magnet. In particular, the shape anisotropy tensor for an ellipsoidal magnet with semiaxis lengths a, b, and c is $\mathbf{K} = \mu_0 M_s^2 \mathbf{N}(a, b, c)$, where $\mathbf{N}(a, b, c)$ depends only on the length ratios a/b and a/c [*Osborn*, 1945].

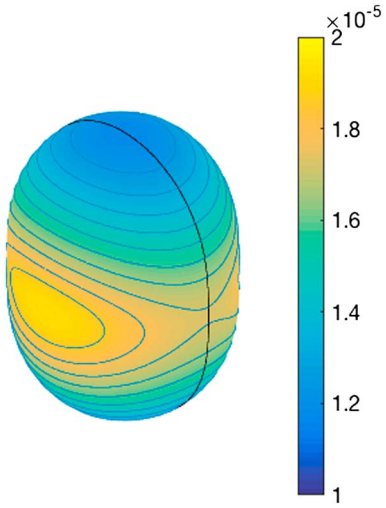

Figure 1. Contours for the normalized energy g (equation (20)) in zero field are plotted on the surface of a magnet with semimajor axes 10 nm, 11 nm, and 15 nm. The line cutting the contours follows the energy gradients from the two saddle points to the two minima (blue regions).

If the unit vectors in the direction of the applied field and the magnetization are $\mathbf{h} = (h_x, h_y, h_z)$ and $\mathbf{m} = (m_x, m_y, m_z)$, the energy is

$$E(\mathbf{m}, H) = V\mathbf{m}^{\mathsf{T}}\mathbf{K}\mathbf{m} - \mu_0 M_s H V \mathbf{h}^{\mathsf{T}}\mathbf{m}. \tag{19}$$

I will choose coordinates so the principal axes are in the x, y, and z directions, so $\mathbf{N}$ is diagonal, and work with the normalized energy density

$$g(\mathbf{m}, \mathcal{H}) = \frac{E(\mathbf{m}, H)}{\mu_0 M_s^2 V} = \mathbf{m}^{\mathsf{T}}\mathbf{N}\mathbf{m} - \mathcal{H}\mathbf{h}^{\mathsf{T}}\mathbf{m}, \tag{20}$$

where $\mathcal{H} = H/M_s$ and

$$\mathbf{N} = \frac{\mathbf{K}}{\mu_0 M_s^2}. \tag{21}$$

An example of the dependence of energy on the direction of magnetization is shown in Figure 1.

The stable states are the two energy minima in the $\pm z$ direction and are connected by two saddle points in the $\pm y$ directions.

The energy minima, saddle points, and maxima are all equilibrium states satisfying $\partial g/\partial \mathbf{m} = 0$ with a constraint $|\mathbf{m}| = 1$ that can be incorporated using Lagrange multipliers. Define

$$g_\lambda(\mathbf{m}, \mathcal{H}) = g(\mathbf{m}, \mathcal{H}) + \lambda\left(\mathbf{m}^{\mathsf{T}}\mathbf{m} - 1\right), \tag{22}$$

and

$$F(\mathbf{m}, \lambda, \mathcal{H}) = \left(\frac{\partial g_\lambda}{\partial m_x}, \frac{\partial g_\lambda}{\partial m_y}, \frac{\partial g_\lambda}{\partial m_z}, \frac{\partial g_\lambda}{\partial \lambda}\right). \tag{23}$$

The equilibrium equations $F(\mathbf{m}, \lambda, \mathcal{H}) = 0$ implicitly define the components of $\mathbf{m}$ as functions of $\mathcal{H}$. The first derivatives $\partial \mathbf{m}(\mathcal{H})/\partial \mathcal{H}$ can be calculated using partial differentiation. The analytical results in the next few sections are obtained using a computer algebra system, Maple 2015 (details are in the supporting information).

Suppose that $N_{xx} \geq N_{yy} \geq N_{zz}$, so the z, y, and x axes are the easy, intermediate, and hard axes. In zero field, these correspond to the energy minima ($\mathbf{m} = (0, 0, \pm 1)$), saddle points ($\mathbf{m} = (0, \pm 1, 0)$), and maxima ($\mathbf{m} = (\pm 1, 0, 0)$). Since the maxima have no influence on the magnetic properties, I will ignore them. In a small field, these states are to first order

$$\mathbf{m} = \begin{cases} \left(\frac{1}{2}\frac{\mathcal{H}h_x}{N_{xx}-N_{zz}}, \frac{1}{2}\frac{\mathcal{H}h_y}{N_{yy}-N_{zz}}, \pm 1\right) & \text{(minima)} \\ \left(\frac{1}{2}\frac{\mathcal{H}h_x}{N_{xx}-N_{yy}}, \pm 1, \frac{1}{2}\frac{\mathcal{H}h_z}{N_{zz}-N_{yy}}\right) & \text{(saddle).} \end{cases} \tag{24}$$

The energies are

$$g(\mathbf{m}) = \begin{cases} \frac{1}{2}N_{zz} \mp h_z\mathcal{H} & \text{(minima)} \\ \frac{1}{2}N_{yy} \mp h_y\mathcal{H} & \text{(saddle).} \end{cases} \tag{25}$$

Strictly speaking, if $\mathcal{H}$ is sufficiently large compared to $|N_{xx} - N_{yy}|$, one of the second pair of states becomes a maximum. For now, I will ignore this case, returning to it in section 5.

3. Relaxation Rates

In the theory described in section 1, there is a single energy maximum between the stable states (energy minima). If there are two saddle points (equation (24)), there are two paths between minima. The relaxation rate for stable state i is

$$\nu_i/\nu_{th} = \exp\left(\chi_0\left(\mathbf{m}_i(\mathcal{H}) - \mathbf{m}_s^{(1)}(\mathcal{H})\right)\cdot\mathbf{h}\right) + \exp\left(\chi_0\left(\mathbf{m}_i(\mathcal{H}) - \mathbf{m}_s^{(2)}(\mathcal{H})\right)\cdot\mathbf{h}\right), \tag{26}$$

where χ_0 is defined in equation (17) and ν_{th} is defined after equation (14). In a static field with constant transition rates, the system relaxes at the rate $\nu = \nu_+ + \nu_-$.

To first order, the above rates are (see the supporting information)

$$\nu_\pm(\mathcal{H}) = \frac{1}{2\tau}\left(1 \mp \chi_0 \mathcal{H} h_z\right) = \frac{1}{2\tau}\left(1 \mp \chi_0 M_s H h_z\right), \tag{27}$$

where

$$\tau = \frac{1}{\nu_+(0) + \nu_-(0)} = \frac{1}{4\nu_{th}} \exp\left(\frac{\left(K_{yy} - K_{zz}\right) V}{k_B T}\right). \tag{28}$$

(K_{xx} does not appear in this expression because it is associated with the energy maxima.)

4. Frequency-Dependent Susceptibility

Inserting the expressions for the energy minima in equation (24) into equation (4) and using $n_+ + n_- = 1$, the time dependence of the magnetization for the triaxial magnet is

$$\mathbf{M}(t) = \left(\frac{\mu_0 M_s^2 H_x}{2\left(K_{xx} - K_{zz}\right)}, \frac{\mu_0 M_s^2 H_y}{2\left(K_{xx} - K_{zz}\right)}, M_s\left(n_+ - n_-\right)\right). \tag{29}$$

The magnetization vector is divided into a thermal (barrier hopping) contribution (the z component) and the pure rotational response characteristic of the SD limit (the other two components).

The populations $n_\pm(t)$ are determined by the rate equation (5). In measurements of the frequency dependence of susceptibility, the field has a time dependence, so the rates $\nu_\pm(h(t))$ are time dependent, as are the magnetization directions $\mathbf{m}_\pm(h(t))$. Then

$$\dot{M}_z = \frac{1}{\tau}\left(M_{eq} - M_z\right), \tag{30}$$

where M_{eq} is defined in equation (6). If the rates $\nu_\pm$ are independent of time, then M_z approaches M_{eq}.

If the field has time dependence given by equation (14) then to first order, equation (27) gives

$$M_{eq} = \chi_0 H_z \exp(i\omega t). \tag{31}$$

Inserting this into equation (30) and solving gives

$$M_z(t) = M_z(0)\exp\left(-\frac{t}{\tau}\right) + \chi_0 H_z \frac{1}{1 + i\omega\tau}\left[\exp(i\omega t) - \exp\left(-\frac{t}{\tau}\right)\right]. \tag{32}$$

(See the supporting information.) Taking the real part,

$$M_z(t) = M_z(0)\exp\left(-\frac{t}{\tau}\right) + \chi_0 H_z \frac{1}{1 + \omega^2\tau^2}\left[\cos\omega t + \omega\tau \sin\omega t - \exp\left(-\frac{t}{\tau}\right)\right]. \tag{33}$$

The first term is the only part that depends on the initial state and can add a bias to the signal that complicates attempts to fit the periodic response. This can be removed by setting the populations in the + and − states equal to each other, in other words, by alternating field or thermal demagnetization. The second term includes an exponential decay, but its starting value is always zero. In the limit $t \gg \tau$,

$$M_i(t) = \chi_{ij}(\omega) H_j(t), \tag{34}$$

where in the principal axis coordinates χ_{ij} is a diagonal matrix:

$$\chi_{ij}(\omega) = \frac{dM_i}{dH_j} = \mathrm{diag}\left(\frac{\mu_0 M_s^2}{2\left(K_{xx} - K_{zz}\right)}\cos\omega t, \frac{\mu_0 M_s^2}{2\left(K_{yy} - K_{zz}\right)}\cos\omega t, \chi_0 \frac{\cos\omega t + \omega\tau \sin\omega t}{1 + \omega^2\tau^2}\right). \tag{35}$$

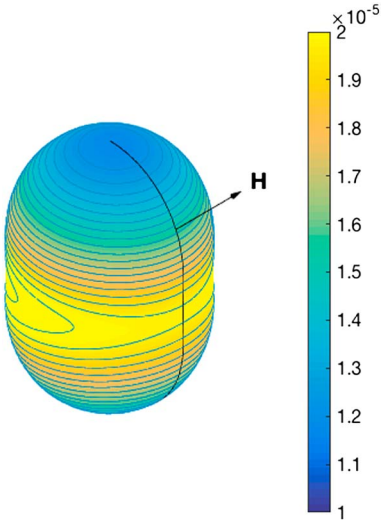

Figure 2. Contours for the normalized energy g (equation (20)) in a field of magnitude 10 mT in the (0, 1, 1) direction are plotted on the surface of a spheroidal magnet with semimajor axes 10 nm, 10 nm, and 15 nm.

The in-phase and quadrature components are the coefficients of the cos ωt and sin ωt terms:

$$\chi'_{ij} = \frac{\mu_0 M_s^2}{2\left(K_{xx} - K_{zz}\right)}\delta_{i1}\delta_{j1} + \frac{\mu_0 M_s^2}{2\left(K_{yy} - K_{zz}\right)}\delta_{i2}\delta_{j2} + \frac{\chi_0}{1+\omega^2\tau^2}\delta_{i3}\delta_{j3}, \tag{36}$$

and

$$\chi''_{ij} = \frac{\chi_0\omega\tau}{1+\omega^2\tau^2}\delta_{i3}\delta_{j3}, \tag{37}$$

where δ_{ij} is the Kronecker delta function.

For a measurement of the magnetization in the direction of the field, the susceptibility is

$$\chi = h_i\chi_{ij}h_j. \tag{38}$$

The in-phase and quadrature components of χ are

$$\chi'(\omega) = \frac{\chi_0 h_z^2}{1+\omega^2\tau^2} + \frac{1}{2}\mu_0 M_s^2\left[\frac{h_x^2}{K_{xx}-K_{zz}} + \frac{h_y^2}{K_{yy}-K_{zz}}\right], \tag{39}$$

and

$$\chi''(\omega) = \frac{\chi_0\omega\tau h_z^2}{1+\omega^2\tau^2}. \tag{40}$$

Given an ensemble of identical particles with isotropically oriented easy axes, since $\langle h_x^2\rangle = \langle h_y^2\rangle = \langle h_z^2\rangle = 1/3$,

$$\langle\chi'(\omega)\rangle_\Omega = \frac{1}{3}\frac{\chi_0}{1+\omega^2\tau^2} + \frac{1}{6}\mu_0 M_s^2\left[\frac{1}{K_{xx}-K_{zz}} + \frac{1}{K_{yy}-K_{zz}}\right], \tag{41}$$

and

$$\langle\chi''(\omega)\rangle_\Omega = \frac{1}{3}\frac{\chi_0\omega\tau}{1+\omega^2\tau^2}, \tag{42}$$

where Ω refers to the surface of a unit sphere.

5. Uniaxial Anisotropy

In the *Stoner and Wohlfarth* [1948] model, the magnetic anisotropy is rotationally symmetric about an axis which I will take to be the z axis. The equation for the energy is equation (12) with $K_u = K_{xx} - K_{zz} = K_{yy} - K_{zz}$. The obvious approach to solving for the susceptibility would be to adapt the triaxial expressions in section 3 to the Stoner-Wohlfarth coordinates. However, in contrast to generic triaxial anisotropy, there is only one energy barrier (Figure 2).

Because of the lack of inversion symmetry in the external field energy, there is an energy saddle point on the forward side and a maximum on the other side. This can also be seen by looking at equation (20) in a rotationally symmetric geometry with the field in the XZ plane. If the magnetization has spherical polar coordinates (Φ, Θ), where Φ is the longitudinal angle and Θ the azimuthal angle, then aside from a constant,

$$g(\Phi,\Theta) = \left(N_{xx} - N_{zz}\right)\cos^2\Theta - \mathcal{H}h_z\cos\Theta - \mathcal{H}h_x\cos\Phi\sin\Theta. \tag{43}$$

For $0 < \Theta \le \pi$ and $h_x > 0$, the energy is a minimum in Φ when $\Phi = 0$ and $\mathcal{H} > 0$ or $\Phi = \pi$ and $\mathcal{H} < 0$. When $\mathcal{H} = 0$, it is independent of Φ. Thus, as the field changes sign, the energy barrier goes from being a saddle point on one side to the entire equator to a saddle point on the other side. This will also occur if there is a small departure from uniaxial anisotropy, but a full analysis is beyond the scope of this article.

Because there is only one energy barrier, the total relaxation time is

$$\tau = \left[\nu_+(0) + \nu_-(0)\right]^{-1} = \frac{1}{2\nu_{th}}\exp\left(\frac{K_u V}{k_B T}\right). \tag{44}$$

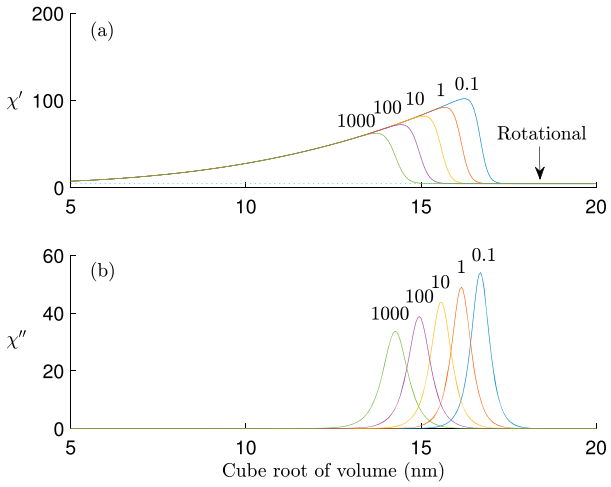

Figure 3. Size dependence of the (a) in-phase and (b) quadrature components of the susceptibility for various frequencies (labeled in Hz) in an isotropic sample containing Stoner-Wohlfarth magnets with aspect ratio 1.5. The dotted line in Figure 3a represents the contribution of rotation.

I will now switch to Stoner-Wohlfarth coordinates in which the energy is given by equation (12). To determine which of the two maxima is a saddle point in spherical coordinates, we can simply take the solution with the lower energy. Taking into account the jump of the saddle point on crossing zero field, a linear expansion of the relaxation rates is as follows (see the supporting information):

$$\tau\nu_{\pm}(H) = \begin{cases} 1 + \chi_0 M_s H(\cos\theta \pm \sin\theta), & H > 0 \\ 1 + \chi_0 M_s H(\sin\theta \pm \cos\theta), & H < 0. \end{cases} \tag{45}$$

For $\nu_{-}(H)$, the coefficient of H is discontinuous at $H = 0$, so the Taylor expansion is not defined at that point. Fortunately, it is defined for the ratio

$$M_{\text{eq}} = \frac{\nu_{-} - \nu_{+}}{\nu_{-} + \nu_{+}} = \chi_0 M_s H \cos\theta + \mathcal{O}(H^2). \tag{46}$$

This is the same as the general triaxial result if $\cos\theta$ is substituted for h_z. Thus, we are justified in adapting the triaxial expressions to uniaxial anisotropy despite the difference in the number of energy barriers. In particular,

$$\chi'(\omega) = \frac{\chi_0}{1 + \omega^2\tau^2}\cos^2\theta + \frac{1}{2}\frac{\mu_0 M_s^2}{K_u}\sin^2\theta, \tag{47}$$

and

$$\chi''(\omega) = \frac{\chi_0\omega\tau}{1 + \omega^2\tau^2}\cos^2\theta. \tag{48}$$

In an isotropic sample, $\langle\cos^2\theta\rangle = 1/3$ and $\langle\sin^2\theta\rangle = 2/3$.

The susceptibility tensors are

$$\chi'_{ij} = \frac{\mu_0 M_s^2}{4K_u}\left(\delta_{i1}\delta_{j1} + \delta_{i2}\delta_{j2}\right) + \frac{\chi_0}{1 + \omega^2\tau^2}\delta_{i3}\delta_{j3}, \tag{49}$$

and

$$\chi''_{ij} = \frac{\chi_0\omega\tau}{1 + \omega^2\tau^2}\delta_{i3}\delta_{j3}. \tag{50}$$

The latter is identical to the expression for triaxial anisotropy.

Equations (47) and (48) agree with those obtained by *Lanci and Zanella* [2016] (their equations (18) and (15) with their ϕ being equivalent to θ here); but their derivation is incorrect. Even the linear expansions of the relaxation rates (equation (45)) are inconsistent with their equation (18). Also, the method of *McNamara and Wiesenfeld* [1989] requires a Taylor expansion for $\nu_{-}(H)$ at H=0, but as we saw above, this is undefined. *Lanci and Zanella* [2016] arrived at the correct result through a fortuitous cancelation of errors.

In the remainder of this article I will discuss applications of these equations for magnets in which the anisotropy is due to particle elongation and the magnets are spheroidal. If a and b are the semimajor and semiminor axes of one of these magnets, and $q = a/b$, then $K_u = \mu_0 M_s^2 N(q)$, where $N(q)$ is a dimensionless demagnetizing factor [*Chikazumi*, 1997]. I represent the size of a magnet by the cube root of the volume instead of the more conventional choice of the longest side. This separates volume effects from shape effects. To get the length of the longest size, multiply by $q^{2/3}$.

In Figure 3 is shown the volume and frequency dependence of the isotropically averaged components of the susceptibility (equations (41) and (42)) for Stoner-Wohlfarth magnets with a shape anisotropy arising from an aspect ratio of 1.5. (All numerical results in this article were calculated using MATLAB 2016a.) In both the in-phase and quadrature components, the peak response occurs at a lower volume (and its height decreases) when the frequency is increased.

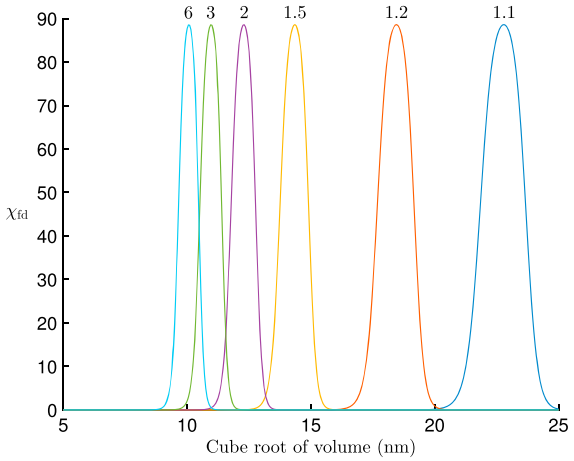

Figure 4. Size dependence of the ratio χ_{fd} for Stoner-Wohlfarth magnets with various aspect ratios.

The quadrature component is sharply peaked, only significantly different from zero over a narrow range of sizes. The in-phase component has a longer tail at low volumes. It closely follows the zero-frequency response until near its peak, then drops off quickly. Near the peak, the thermal contribution is much larger than the rotational contribution.

The ratio χ_{fd}, using the standard frequencies of 470 Hz and 4700 Hz, is plotted in Figure 4 for various aspect ratios. In the thermal contributions, the anisotropy determines the volume dependence of τ through equation (28) and therefore the location of the peak in a plot of χ' against volume. The amplitude of the peak is determined by the direction of the field and the factor $\chi_0 = \mu_0 M_s^2 V/k_B T$. The zero-frequency response common to both frequencies is eliminated from the numerator, resulting in a sharper peak (although not as sharp as χ'').

The heights of the peaks are between 88.5 and 88.6 and almost independent of magnet shape.

6. Relation to Bulk Anisotropy

Equations (39) and (47) show that for a single magnet, the thermal and rotational parts of the susceptibility have opposite anisotropies, with the thermal part peaking on the easy axis while the rotational part peaks in the plane perpendicular to this axis. However, to determine the resulting anisotropy of samples with many such magnets, we must also consider the distribution of magnet orientations. As an obvious example, isotropically distributed Stoner-Wohlfarth magnets have no net anisotropy, regardless of the individual anisotropies.

Consider an arbitrarily oriented Stoner-Wohlfarth magnet in some body. Let the orientation of the symmetry axis be represented by the unit vector **c** and suppose that **a** and **b** are two arbitrary vectors perpendicular to each other and **c**. Suppose that χ^p is the susceptibility tensor in principal axis coordinates. Then, in the coordinates of the body,

$$\chi^b = \mathbf{R}^T \chi^p \mathbf{R}, \tag{51}$$

where $\boldsymbol{R} = [\mathbf{a}, \mathbf{b}, \mathbf{c}]$ has columns corresponding to the principal axes.

Suppose that we have a collection of identical but randomly oriented magnets and that in spherical coordinates, the probability of an axis falling within a given element of surface area dS is $\rho(\Theta, \Phi)\,\mathrm{d}S$, where Θ is the azimuthal angle and Φ the longitudinal angle. (The function ρ is a probability density element [*Fisher et al.*, 1987, pp. 66–67] and should not be confused with a probability density function.) The susceptibility of the body is the mean of χ^b over the surface of a unit sphere:

$$X_{ij} = \langle \chi_{ij}^b \rangle_S = \int_0^{2\pi} \mathrm{d}\Phi \int_0^{\pi} \chi_{ij}^b(\Theta, \Phi) \rho(\Theta, \Phi) \sin\Theta \mathrm{d}\Theta. \tag{52}$$

Substituting equation (50) into (51) gives $\chi_{ij}^b = c_i c_j$ (an outer product of **c** with itself). Therefore,

$$X_{ij}^{b\prime\prime} = \frac{\chi_0 \omega\tau}{1+\omega^2\tau^2} \langle c_i c_j \rangle_S. \tag{53}$$

Equation (49) can be rewritten

$$\chi_{ij}^{p\prime} = \frac{\mu_0 M_s^2}{2K_u}\delta_{ij} + \left(\frac{\chi_0}{1+\omega^2\tau^2} - \frac{\mu_0 M_s^2}{2K_u}\right)\delta_{i3}\delta_{j3}, \tag{54}$$

so

$$X_{ij}^{b\prime} = \frac{\mu_0 M_s^2}{2K_u}\delta_{ij} + \left(\frac{\chi_0}{1+\omega^2\tau^2} - \frac{\mu_0 M_s^2}{2K_u}\right)\langle c_i c_j \rangle_S. \tag{55}$$

Therefore, if the thermal part dominates, X'_{ij} has an SP-like anisotropy, while if the rotational part dominates, it has the opposite anisotropy.

Since an axis orientation can be defined by either of two opposite directions, the probability distribution needs to be a bipolar one such as the Watson or Bingham distributions [*Fisher et al.*, 1987, pp. 89–92 and 97]. For a more physically motivated distribution, consider the "line/plane" model of deformation of rocks, in which magnetic minerals rotate but do not change shape [*Hrouda*, 1993]. This is known as the March model in structural geology [*March*, 1932; *Owens*, 1973].

Mulchrone and Talbot [2016] derived an angular probability distribution for finite deformations in which a position vector before and after deformation is related by a matrix **S**:

$$\mathbf{r}_\mathrm{f} = \mathbf{S}\mathbf{r}_\mathrm{i}. \tag{56}$$

They chose coordinates in which **S** is diagonal and constrained S_{22} so the volume does not change:

$$S_{ij} = S_1\delta_{i1}\delta_{j1} + \left(S_1S_3\right)^{-1}\delta_{i2}\delta_{j2} + S_3\delta_{i3}\delta_{j3}. \tag{57}$$

If this is applied to an initially isotropic solid,

$$\rho\left(\Theta,\Phi\right)\mathrm{d}S = \frac{1}{4\pi}\lambda^{3/2}\mathrm{d}S, \tag{58}$$

where

$$\lambda = \frac{S_1^2S_3^2}{S_1^2\cos^2\Theta + S_3^2\cos^2\Phi\sin^2\Theta + S_1^4S_3^4\sin^2\Phi\sin^2\Theta}. \tag{59}$$

If $S_1 = S_3 = 1$, the solid is not deformed.

Because of the symmetries of ρ, the off-diagonal products of c_ic_j have zero mean, so X'_{ij} and X''_{ij} are diagonal. For small strains, we can approximate S_{ij} by $\delta_{ij} + e_{ij}$, where e_{ij} is the infinitesimal strain tensor. Inserting this in equation (57) gives

$$e_{ij} = e_{11}\delta_{i1}\delta_{j1} - \left(e_{11} + e_{33}\right)\delta_{i2}\delta_{j2} + e_{33}\delta_{i3}\delta_{j3}. \tag{60}$$

Expanding ρ in e_1 and e_3 and integrating over the sphere gives (see the supporting information)

$$\langle c_ic_j\rangle_S \approx \frac{1}{3}\delta_{ij} + \frac{2}{5}e_{ij}, \tag{61}$$

Therefore,

$$X'_{ij} \approx \frac{\mu_0M_\mathrm{s}^2}{2K_\mathrm{u}}\delta_{ij} + \left(\frac{\chi_0}{1+\omega^2\tau^2} - \frac{\mu_0M_\mathrm{s}^2}{2K_\mathrm{u}}\right)\left(\frac{1}{3}\delta_{ij} + \frac{2}{5}e_{ij}\right). \tag{62}$$

and

$$X''_{ij} \approx \frac{\chi_0\omega\tau}{1+\omega^2\tau^2}\left(\frac{1}{3}\delta_{ij} + \frac{2}{5}e_{ij}\right). \tag{63}$$

These approximations are accurate to 2% for strains up to 10%. Although they were derived in a particular coordinate system, they are expressed in terms of second order tensors, so the relationships hold in any coordinate system.

Compared to $S_{ij} = \delta_{ij} + e_{ij}$, X''_{ij} underestimates the deformation. However, we can use the fact that e_{ij} has zero trace to isolate it and correct the proportion:

$$S_{ij} \propto S''_{ij} = \frac{1}{3}\mathrm{Tr}\left(X''_{ij}\right) + \frac{5}{2}\left(X''_{ij} - \frac{1}{3}\mathrm{Tr}\left(X''_{ij}\right)\right). \tag{64}$$

The in-phase component has an anisotropy that can vary depending on the relative strength of the thermal and rotational contributions. In a sample dominated by stable SD magnets, it has the opposite anisotropy to the quadrature component. If a *Henkel* [1964] plot or *Cisowski* [1981] test indicate that the sample is indeed dominated by stable SD magnets, then the strain anisotropy can be estimated using the following parameter:

$$S_{ij} \propto S'_{ij} = \frac{1}{3}\mathrm{Tr}\left(X'_{ij}\right) - \frac{5}{2}\left(X'_{ij} - \frac{1}{3}\mathrm{Tr}\left(X'_{ij}\right)\right). \tag{65}$$

7. Locations of Peak Frequencies

In one model for χ_{fd} [*Dearing et al.*, 1996], the ratio χ_{fd} was assumed to reach a maximum at the SP/SD boundary for a time scale of $t = 1/\omega$, then decrease linearly to zero at the SP/SD boundary for $t = 100$ s. Thus, the authors assumed that the peak lay in the SP region. We will now determine the relationship between the peak and the SP/SD boundary.

In all magnets with triaxial anisotropy (equations (39) and (40)), the susceptibility depends on volume both directly and indirectly through the relaxation time τ (equation (28)). The volume-dependent parts are

$$\frac{V}{1+\omega^2\tau(V)^2} = \frac{V}{1+w^2\exp(2bV)}. \tag{66}$$

for the in-phase component, and

$$\frac{V\omega\tau(V)}{1+\omega^2\tau(V)^2} = \frac{Vw\exp(bV)}{1+w^2\exp(2bV)} \tag{67}$$

for the quadrature component. Here I have defined

$$w = \frac{\omega}{4v_{th}} \tag{68}$$

$$b = \frac{K_{yy} - K_{zz}}{k_B T}. \tag{69}$$

For uniaxial anisotropy (equations (44), (47), and (48)),

$$w = \frac{\omega}{2v_{th}} \tag{70}$$

$$b = \frac{K_u}{k_B T}. \tag{71}$$

These factors are independent of field direction.

The in-phase factor (and therefore χ') has a maximum at

$$v_{peak} = \frac{1}{2b}\left[W\left(\frac{1}{ew^2}\right) + 1\right], \tag{72}$$

where $W(x)$ is the Lambert W function for real numbers [*Corless et al.*, 1996]. The location of the maximum for χ'' must be found numerically.

Substituting $\tau = 1/\omega$ in equation (28) or (44), the critical volume is

$$v_{sp}\left(\frac{1}{\omega}\right) = -\frac{1}{b}\ln w. \tag{73}$$

Thus, for the in-phase component,

$$\frac{v_{peak}}{v_{sp}}(\omega) = -\frac{W\left(1/ew^2\right)+1}{2\ln w}. \tag{74}$$

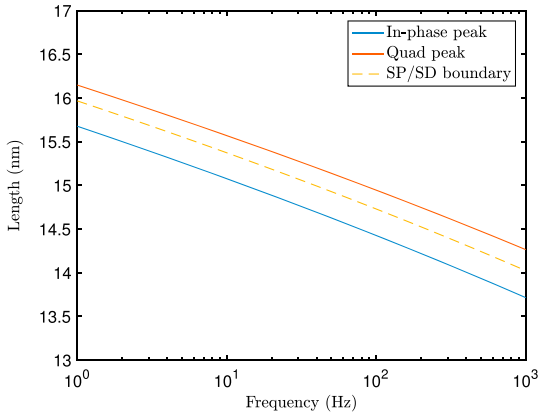

Figure 5. Susceptibility peaks as a function of frequency ω for an aspect ratio of 1.5. The SP/SD critical size for time scale $1/\omega$ is included for comparison.

This ratio does not depend on the aspect ratio q or on temperature (unless the prefactor ν_{th} depends on temperature).

The frequency dependence of the susceptibility peaks is shown in Figure 5. For comparison, the SP/SD critical size is shown for a time scale of $1/\omega$. The peaks bracket this critical size and are at nearly constant multiples of 1.013 ± 0.003 for the quad peaks and 0.980 ± 0.003 for the in-phase peaks.

8. Volume Averages

The thermal and rotational parts of the susceptibility have opposing anisotropies: when h_z^2 is large, h_x^2 and h_y^2 are small. If the SP fraction dominates, it can be distinguished from an SD sample by the ipAMS. However, the peaks in Figure 3 are narrow, so it will only dominate in a volume distribution that is tightly concentrated around them.

Suppose that $\rho(V)$ is a volume distribution such that

$$\int_0^\infty \rho(V)\mathrm{d}V = 1. \tag{75}$$

The volume-average susceptibility is the weighted average

$$\langle\chi\rangle_v = \frac{1}{V_{tot}}\int_0^\infty V\rho(V)\chi(V)\mathrm{d}V, \tag{76}$$

where

$$V_{tot} = \int_0^\infty V\rho(V)\mathrm{d}V \tag{77}$$

is the total volume of the magnets. The relaxation rate $\tau(V)$ being volume-dependent, the average susceptibilities are

$$\begin{aligned}\chi'(\omega) =& \chi_0 h_z^2\left\langle\frac{V}{1+\omega^2\tau(V)^2}\right\rangle_V \\ &+ \mu_0 M_s^2\left[\frac{h_x^2}{K_{xx}-K_{zz}} + \frac{h_y^2}{K_{yy}-K_{zz}}\right],\end{aligned} \tag{78}$$

and

$$\chi''(\omega) = \chi_0 h_z^2\left\langle\frac{V\omega\tau(V)}{1+\omega^2\tau(V)^2}\right\rangle_V. \tag{79}$$

Suppose the lengths have a lognormal distribution:

$$\rho(x;\mu,\sigma) = \frac{1}{x\sigma\sqrt{2\pi}}\exp\left(\frac{-(\ln x-\mu)^2}{2\sigma^2}\right) \tag{80}$$

for parameters μ and σ. The corresponding distribution for the volume $V = x^3$ is $\rho(V; 3\mu, 3\sigma)$.

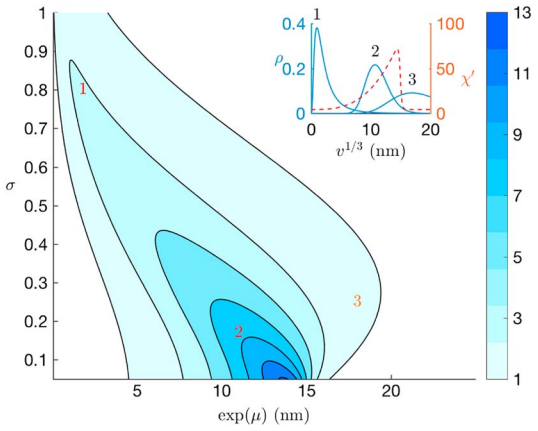

Figure 6. Ratio of thermal to rotational part of χ' as a function of the lognormal volume distribution parameters μ and σ. The magnets have aspect ratio $q = 1.5$ and the frequency of the field is $\omega = 100$ Hz. Inset: Volume distributions for the three numbered points in the contour plot. The single-magnet size dependence of χ' for this frequency is plotted as a dashed line for comparison.

In Figure 6 is plotted the ratio between the thermal and rotational parts of the in-phase component χ' for a frequency $\omega = 100$ Hz. The blue region represents the volume distributions that can have an inverse anisotropy. Almost all of it is below 18.2 nm, the size of maximum susceptibility for this frequency; and as the spread of the distribution increases, the center decreases.

To understand the leftward sweeping shape of this curve, I plot some representative distributions in the inset to Figure 6, along with $\chi'\left(V^{1/3}\right)$ for this frequency

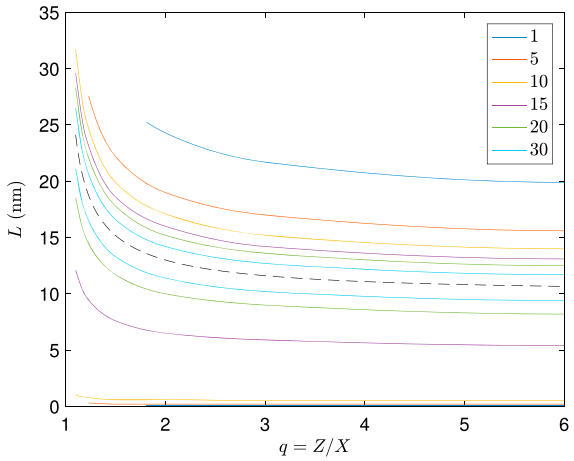

Figure 7. Upper and lower bounds of $L = \exp(\mu)$ as a function of the aspect ratio q. The legend gives the value of χ_{fd}. The dashed line is the SP/SD boundary for a time scale of 0.1 s.

($\chi'(V)$ is used in equation (76)). The thermal contribution is greater than the rotational contribution between 5.8 nm and 15.3 nm. A distribution can be predominantly below this span (as in Example 1) and still have a negative anisotropy if there is a tail in the region. On the other end, curve 3 is near the edge of the region where the thermal contribution dominates; despite the lower susceptibility, the magnets to the right of the peak dominate the signal because their volumes are greater.

By contrast with the in-phase component, the quadrature component only has a thermal contribution, so it should always have a maximum parallel to the easy axis. It is a weaker signal than the in-phase component, but it is pure, and the peaks are narrower since they lack the zero-frequency contribution.

Under some conditions, the ratio χ_{fd} can be used to place constraints on the size distribution. For a given aspect ratio q, a contour plot like Figure 6 can be constructed for χ_{fd} and constraints put on the size distribution parameters for a given value. The region where $\chi_{fd} > 5\%$ largely coincides with the region of positive anisotropy in Figure 6. Plots for different values of q look similar but are shifted as in Figure 4. However, Stoner-Wohlfarth theory is only applicable if the magnetization is almost entirely coming from Stoner-Wohlfarth magnets. For shape anisotropy, the upper bound on the size is given by

$$L_{SW}^{coerc} = q^{1/3} \left(\frac{A}{\mu_0 M_s^2} \right)^{1/2} \left(\frac{k}{N_{xx}} \right)^{1/2}, \tag{81}$$

where A is the exchange constant and $k = 20$ to within 7% [*Newell and Merrill*, 1999]. (This size is independent of the cubic anisotropy as long as the elongation is in a ⟨001⟩ or ⟨111⟩ crystallographic direction.) In a lognormal distribution, 95% of the probability lies within the size interval $[\exp(\mu - 2\sigma), \exp(\mu + 2\sigma)]$, so a reasonable criterion for the applicability of the theory is $L_{max} = \exp(\mu + 2\sigma) < L_{SD}^{coerc}$.

In Figure 7, upper and lower bounds of $\exp(\mu)$ (the location of the peak in the size distribution) are shown for various values of χ_{fd}. As this ratio decreases below about 5%, the lowest value of q for which Stoner-Wohlfarth theory applies starts to climb, so any interpretation comes with caveats. There is little constraint on the lower bound until $\chi_{fd} > 10$, but even for $\chi_{fd} = 1$ there is an upper size limit that is only about twice the SP/SD boundary. A ratio of 30%, as in the Yucca Mountain Tuffs, puts a tight constraint on the location of the peak.

9. Discussion

9.1. Size Dependence

The parameter χ_{fd} (equation (1)) is a good indicator of a population of magnets with sizes concentrated near the SP/SD boundary. It has an upper limit of 88.6% and becomes negligible within about 3 nm of the peak. There is no evidence of a significant frequency dependence in the susceptibility of magnets above the SD size range, so the numerator of χ_{fd} probably provides information only on the magnets near the SP/SD boundary. However, the denominator χ'_{lf} includes the susceptibility of any non-SD magnets.

Even in a sample with only SD magnets of a particular shape, an inversion for the size distribution is nonunique. Figure 6 illustrates this problem. The contours are for a normalized value of χ' (the rotational part being a constant). If the size distribution is assumed to be lognormal, there are only two distribution parameters that determine χ'. Nevertheless, for a given value of χ', the possible combinations of μ and σ lie on a curve, so the best we can do is place bounds on them.

In a preliminary attempt to constrain the size distribution, I looked at the bounds on μ as a function of aspect ratio (Figure 7). Such bounds can only be determined if Stoner-Wohlfarth theory applies across the entire size distribution, so small values of χ_{fd} cannot place unambiguous constraints on the size. However, for values of 10% or greater, a clear result is obtained, limiting the location of the peak to below about 32 nm even in a sample with mixed shapes. In addition, at least 95% of the magnets are well below the critical size for single-domain switching (equation (81)). For values of 15% or greater, there is also a tight constraint on the lower bound.

The calculations in Figure 7 are for magnetite at room temperature. The relationship between the peak response of each magnet and the SP/SD boundary is robust, being independent of elongation and weakly

dependent of temperature or composition, so it would be easy to scale them to other temperatures. However, the upper critical size L_{coerc} has a quite different dependence on temperature from the SP/SD critical size, so it would be necessary to check that the size distribution still falls below it.

Contributions from non-SD magnets add only to the denominator of χ_{fd}, lowering its value, so a value of 10% or above provides robust upper bounds on the SD population; any non-SD contamination would occur because the size distribution is multimodal or there are other compositions in the sample. An inversion for both size and shape may be feasible for Stoner-Wohlfarth magnets if both components of the susceptibility are included for varying frequency and temperature. This provides information on two functions, $\chi'(\omega, T)$ and $\chi''(\omega, T)$, for a four-dimensional data set. In equations (47) and (48), there are three temperature-dependent parameters: $\chi_0 = \mu_0 M_s V / k_B T$, $\beta = \mu_0 M_s^2 / K_u$, and $\omega\tau$. Since ω is known and $\tau = \exp(\chi_0/\beta)/2\nu_{th}$, these parameters depend on K_u, V, ν_{th}, and M_s. If M_s can be determined from compositional information, this leaves an overdetermined inversion for three parameters.

For aligned magnets, *Shcherbakov and Fabian* [2005] consider a joint distribution $\rho(V, \epsilon)$ of volumes and energy barriers. They find a dispersion relation linking the averaged in-phase and quadrature components:

$$\mathcal{F}\left[\chi''\right](y) = i \tanh(\pi y) \mathcal{F}\left[\chi'\right](y), \tag{82}$$

where

$$\mathcal{F}[h](y) \equiv \int_{-\infty}^{\infty} h(x) \exp(-ixy) dx \tag{83}$$

is the Fourier transform of a function h.

In systems of randomly oriented triaxial or uniaxial samples, the expressions for the thermal part of the susceptibility (e.g., equations (39) and (40)) are multiplied by the same directional factor (either h_z for triaxial or $\cos^2\theta$ for uniaxial particles), so the dispersion relation still holds. However, the in-phase component also has a rotational contribution χ_{rot} that does not depend on frequency or volume. Thus, in expressions involving Fourier transforms of the susceptibility, e.g., their equation (24), χ_p must be replaced by $\chi' - \chi_{rot}$.

Having obtained an expression for the effective volume $\overline{V}(\epsilon)d\epsilon$ of magnets with energy barriers between ϵ and $\epsilon + d\epsilon$, *Shcherbakov and Fabian* [2005] show how to invert susceptibility measurements to obtain $\overline{V}(\epsilon)$ by fitting the in-phase and quadrature components to polynomials (their equation (28) with a regularizing factor that is then replaced by its limit of 1). With an additional assumption about the energy barriers, the volume distribution $\rho(V, \epsilon)$ can be obtained. Unfortunately, the zero-order term in the expansion of $\chi'_{th}(\omega)$ is independent of frequency, so it may not be possible to separate it from χ_{rot} without further information such as the value of M_s.

In addition to the ambiguity in the rotational part, there is the more general problem of nonuniqueness discussed above. This problem only increases since there is one dimension of variability for each term in the expansion of $\chi'_{th}(\omega)$. Contamination from non-SD susceptibility is also a significant problem. I approached this problem by placing bounds on the size distribution, and a generalization of this approach may also be appropriate for inversions of temperature/frequency data.

In this manuscript I have treated ν_{th}, the preexponential factor in Néel theory, as a constant. However, this may not be adequate in temperature-dependent inversions, since it is actually a variable that depends on the shape of the energy surface near the minima and transition state as well as a gyromagnetic factor and a damping constant [*Brown*, 1979]. It also depends on the magnetic field, so it is not obvious that the linearization used in this article can be extended to the variability in ν_{th}.

One of the great advantages of using the frequency dependence of susceptibility to investigate size distributions in the SP/SD size range is that it is minimally sensitive to larger magnets. However, magnetostatic interactions between magnets can modify the response, introducing errors into the inversion. A common approach to magnetostatic interactions is to represent them by a mean interaction field [e.g., *Dormann et al.*, 1988; *Mørup and Tronc*, 1994]. In applying mean field models to superparamagnetic systems, there is controversy over how to handle particles of different sizes [*Hansen and Mørup*, 1998; *Dormann et al.*, 1999]; but all the mean field models are essentially single-domain models in which the system is treated as if it has a single energy barrier shifted by the mean field. In reality, magnetostatic interactions can be expected to greatly increase the number of energy barriers [*Newell*, 2009]. For now, the use of frequency-dependent

susceptibility is most reliable if a *Henkel* [1964] plot or *Cisowski* [1981] test confirms that interactions are negligible.

9.2. Anisotropy

Above, I discussed inverting for size distributions when a sample is isotropic. Can the analysis be extended to anisotropic samples? In general, anisotropy mixes the thermal and rotational contributions (equation (55)) and introduces new variables such as the strain. In the March model with the constraint that the volume is unchanged, these contributions can be unmixed. Taking the trace of the tensors in equations (62) and (63) and using $\mathrm{Tr}(e_{ij}) = 0$ gives

$$\mathrm{Tr}\left(X'_{ij}\right) = \frac{\mu_0 M_s^2}{K_u} + \frac{\chi_0}{1+\omega^2\tau^2} \tag{84}$$

$$\mathrm{Tr}\left(X''_{ij}\right) = \frac{\chi_0 \omega\tau}{1+\omega^2\tau^2}. \tag{85}$$

In the March model, the angular distribution of easy axes does not depend on magnet size and shape, so the size analysis can proceed in the same way as for isotropic solids using the above expressions.

In the study of magnetic anisotropy, there are four models for the effect of deformation on magnetic minerals, known as the "passive," "ductile," "line/plane," and "viscous" models [*Hrouda*, 1993]. The latter two treat the magnets as rigid bodies that rotate in response to deformation; in the line/plane model (synonymous with the March model that I have analyzed in this article), the rotation does not depend on particle shape, but in the viscous model it does. This complicates the analysis of anisotropy in a sample with varying particle shape. The other two models involve deformation of the magnets themselves. None of these models assume any dependence of anisotropy on magnet size.

If the anisotropy is measured for tectonic and environmental applications, we have the complementary problem of separating the strain tensor from the magnetic parameters:

$$X'_{ij} - \frac{1}{3}\mathrm{Tr}\left(X'_{ij}\right)\delta_{ij} \approx \frac{2}{5}\left(\frac{\chi_0}{1+\omega^2\tau^2} - \frac{\mu_0 M_s^2}{2K_u}\right)e_{ij} \tag{86}$$

$$X''_{ij} - \frac{1}{3}\mathrm{Tr}\left(X''_{ij}\right)\delta_{ij} \approx \frac{2}{5}\frac{\chi_0\omega\tau}{1+\omega^2\tau^2}e_{ij}. \tag{87}$$

To determine the absolute strains, we would need to invert for the magnetic parameters and distribution of volumes and shapes. However, for many purposes equations (64) and (64) can lead to improved anisotropy parameters involving ratios between strain components. The parameter S'_{ij} would be preferred if the sample is predominantly stable SD, while S''_{ij} is best if there is a significant population near the SP/SD transition.

Like χ'', thermoremanent magnetization (TRM) is determined by barrier hopping and is aligned with the easy axis of each magnet. Thus, it has the same anisotropy. The quadrature component is therefore a good alternative to using remanence anisotropy for corrections to the paleomagnetic field direction. Compared to remanence, it has the advantage that it picks out only the magnets near the SP/SD boundary, and SD magnets are the most reliable carriers of TRM. An analysis similar to that used in this article could be used to determine the low-field expansion of TRM and its anisotropy. If methods can be developed to resolve the ambiguities in size and shape distribution that were described in the previous section, the distribution can be used to analyze the acquisition of TRM in a given sample.

In applying the expressions for frequency-dependent susceptibility to size and angular distributions, I have concentrated on rotationally symmetric (Stoner-Wohlfarth) magnets whose response is given by equations (47) and (48). If the more general triaxial expressions (equations (39) and (40)) are used, there is an additional anisotropy parameter to determine and the orientations of all three principal axes are needed. An appropriate generalization of the spherical polar coordinate system would be Euler angles. It will be necessary to generalize physical models like that of *Mulchrone and Talbot* [2016] to handle this extra complexity.

Acknowledgments
Supporting data are available from the corresponding author (andrew_newell@ncsu.edu). This work was supported by National Science Foundation grant EAR-1417095.

References

Borradaile, G. J., and M. A. Puumala (1989), Synthetic magnetic fabrics in a plasticene medium, *Tectonophysics*, *164*, 73–78.
Brown, W. F., Jr. (1979), Thermal fluctuations of fine ferromagnetic particles, *IEEE Trans. Magn.*, *15*, 1196–1208.
Chikazumi, S. (1997), *Physics of Ferromagnetism*, 655 pp., Oxford, New York.
Cisowski, S. (1981), Interacting vs. non-interacting single domain behavior in natural and synthetic samples, *Phys. Earth Planet. Inter.*, *26*, 56–62.

Corless, R. M., G. H. Gonnet, D. E. G. Hare, D. J. Jeffrey, and D. E. Knuth (1996), On the LambertW function, *Adv. Comput. Math.*, *5*(1), 329–359, doi:10.1007/BF02124750.

Dearing, J. A., R. J. L. Dann, K. Hay, J. A. Lees, P. J. Loveland, B. A. Maher, and K. O'Grady (1996), Frequency-dependent susceptibility measurements of environmental materials, *Geophys. J. Int.*, *124*, 228–240.

Dormann, J., L. Bessais, and D. Fiorani (1988), A dynamic study of small interacting particles: Superparamagnetic model and spin-glass laws, *J. Phys. C*, *21*, 2105–2034.

Dormann, J., D. Fiorani, and E. Tronc (1999), On the models for interparticle interactions in nanoparticle assemblies: Comparison with experimental results, *J. Magn. Magn. Mater.*, *202*, 251–267.

Dunlop, D. J. (1965), Grain distributions in rocks containing single domain grains, *J. Geomagn. Geoelectr.*, *17*(3–4), 459–471.

Dunlop, D. J. (1986), Coercive forces and coercivity spectra of submicron magnetites, *Earth Planet. Sci. Lett.*, *78*, 288–295.

Egli, R. (2004a), Characterization of individual rock magnetic components by analysis of remanence curves. 2. Fundamental properties of coercivity distributions, *Phys. Chem. Earth Part A.*, *29*(13–14), 851–867.

Egli, R. (2004b), Characterization of individual rock magnetic components by analysis of remanence curves. 3. Bacterial magnetite and natural processes in lakes, *Phys. Chem. Earth Part A.*, *29*(13–14), 869–884.

Egli, R. (2009), Magnetic susceptibility measurements as a function of temperature and frequency I: Inversion theory, *Geophys. J. Int.*, *177*(2), 395–420.

Egli, R., A. P. Chen, M. Winklhofer, K. P. Kodama, and C.-S. Horng (2010), Detection of noninteracting single domain particles using first-order reversal curve diagrams, *Geochem. Geophys. Geosyst.*, *11*, Q01Z11, doi:10.1029/2009GC002916.

Evans, M. E., and F. Heller (2003), *Environmental Magnetism: Principles and Applications of Enviromagnetics*, 299 pp., Academic Press, San Diego, Calif.

Eyre, J. K. (1997), Frequency dependence of magnetic susceptibility for populations of single-domain grains, *Geophys. J. Int.*, *129*(1), 209–211.

Fisher, N. I., T. Lewis, and B. J. J. Embleton (1987), *Statistical Analysis of Spherical Data*, Cambridge Univ. Press, Cambridge, New York.

García-Palacios, J. L. (2000), On the statics and dynamics of magnetoanisotropic nanoparticles, *Adv. Chem. Phys.*, *112*, 1–210.

Hansen, M., and S. Mørup (1998), Models for the dynamics of interacting magnetic nanoparticles, *J. Magn. Magn. Mater.*, *184*, 262–274.

Henkel, O. (1964), Remanenzverhalten und Wechselwirkungen in hartmagnetischen Teilchenkollektiven,*Phys. Stat. Sol.*, *7*, 919–929.

Hrouda, F. (1993), Theoretical models of magnetic anisotropy to strain relationship revisited, *Phys. Earth Planet. Inter.*, *77*, 237–249.

Hrouda, F., and J. Ježek (2017), Role of single-domain magnetic particles in creation of inverse magnetic fabrics in volcanic rocks: A mathematical model study, *Stud. Geophys. Geod.*, *61*(1), 145–161, doi:10.1007/s11200-015-0675-6.

Hrouda, F., M. Chadima, J. Ježek, and J. Pokorný (2017), Anisotropy of out-of-phase magnetic susceptibility of rocks as a tool for direct determination of magnetic subfabrics of some minerals: An introductory study, *Geophys. J.*, *208*, 385–402.

Jackson, M., B. Carter-Stiglitz, R. Egli, and P. Solheid (2006), Characterizing the superparamagnetic grain distribution $f(v, h_k)$ by thermal fluctuation tomography, *J. Geophys. Res.*, *111*, B12S07, doi:10.1029/2006JB004514.

Janák, F. (1967), The effect of the anisotropy of magnetic susceptibility on the direction of the vector of isothermal remanent magnetic polarization, *Stud. Geophys. Geod.*, *11*(4), 419–429, doi:10.1007/BF02589593.

Kirschvink, J. L., and M. M. Walker (1985), Particle-size considerations for magnetite-based magnetoreceptors, in *Magnetite Biomineralization and Magnetoreception in Organisms: A New Biomagnetism*, edited by J. Kirschvink, D. Jones, and B. MacFadden, pp. 243–254, Plenum Press, New York.

Lanci, L., and E. Zanella (2016), The anisotropy of magnetic susceptibility of uniaxial superparamagnetic particles: Consequences for its interpretation in magnetite and maghemite bearing rocks, *J. Geophys. Res. Solid Earth*, *121*, 27–37, doi:10.1002/2015JB012255.

Liu, Q., J. Torrent, B. A. Maher, Y. Yu, C. Deng, R. Zhu, and X. Zhao (2005), Quantifying grain size distribution of pedogenic magnetic particles in Chinese loess and its significance for pedogenesis, *J. Geophys. Res.*, *110*(B11102), doi:10.1029/2005JB003726.

Liu, Q., A. P. Roberts, J. C. Larrasoaña, S. K. Banerjee, Y. Guyodo, L. Tauxe, and F. Oldfield (2012), Environmental magnetism: Principles and applications, *Rev. Geophys.*, *50*, RG4002, doi:10.1029/2012RG000393.

March, A. (1932), Mathematische theorie der regelung nach der korngestah bei affiner deformation, *Z. Kristallogr. – Cryst. Mater.*, *81*(1–6), 285–297.

Martín-Hernández, F., and E. C. Ferré (2007), Separation of paramagnetic and ferrimagnetic anisotropies: A review, *J. Geophys. Res.*, *112*, B103105, doi:10.1029/2006JB004340.

Mayergoyz, I. D. (1991), *Mathematical Models of Hysteresis*, 207 pp., Springer, New York.

McCabe, C., M. Jackson, and B. Ellwood (1985), Magnetic anisotropy in the Trenton limestone: Results of a new technique, anisotropy of anhysteretic susceptibility, *Geophys. Res. Lett.*, *12*, 333–336.

McNamara, B., and K. Wiesenfeld (1989), Theory of stochastic resonance, *Phys. Rev. A*, *39*(9), 4854–4869.

Mørup, S., and E. Tronc (1994), Superparamagnetic relaxation of weakly interacting particles, *Phys. Rev. Lett.*, *72*(20), 3278–3281.

Mulchrone, K. F., and C. J. Talbot (2016), Strain estimation in 3D by fitting linear and planar data to the March model, *Tectonophysics*, *686*, 63–67.

Mullins, C. E., and M. S. Tite (1973), Magnetic viscosity, quadrature susceptibility, and frequency dependence of susceptibility in single-domain assemblies of magnetite and maghemite, *J. Geophys. Res.*, *78*(5), 804–809, doi:10.1029/JB078i005p00804.

Néel, L. (1949), Théorie du traînage magnétique des ferromagnétiques en grains fins avec application aux terres cuites, *Ann. Géophys.*, *5*, 99–136. translated in Nicholas Kurti, editor, Selected Works of Louis Néel, Gordon and Breach, New York, 1988, 407–427.

Newell, A. J. (2000), The Lowrie-Fuller test: Single-domain and micromagnetic theory, *Earth Planet. Sci. Lett.*, *183*(1–2), 335–346, doi:10.1016/S0012-821X(00)00271-5.

Newell, A. J. (2005), A high-precision model of first-order reversal curve (FORC) functions for single-domain ferromagnets with uniaxial anisotropy, *Geochem. Geophys. Geosyst.*, *6*, Q05010, doi:10.1029/2004GC000877.

Newell, A. J. (2009), Transition to superparamagnetism in chains of magnetosome crystals, *Geochem. Geophys. Geosyst.*, *10*, Q11Z08, doi:10.1029/2009GC002538.

Newell, A. J., and R. T. Merrill (1999), Single-domain critical sizes for coercivity and remanence, *J. Geophys. Res.*, *104*, 617–628.

Newell, A. J., and R. T. Merrill (2000), Nucleation and stability of remanent states, *J. Geophys. Res.*, *105*, 19,377–19,391.

Osborn, J. (1945), Demagnetizing factors of the general ellipsoid, *Phys. Rev.*, *67*(11–12), 351–357.

Owens, W. (1973), Strain modification of angular density distributions, *Tectonophysics*, *16*(3), 249–261, doi:10.1016/0040-1951(73)90014-0.

Pike, C. R., A. P. Roberts, and K. L. Verosub (1999), Characterizing interactions in fine magnetic particle systems using first order reversal curves, *J. Appl. Phys.*, *85*, 6660–6667.

Potter, D. K., and A. Stephenson (1988), Single-domain particles in rocks and magnetic fabric analysis, *Geophys. Res. Lett.*, *15*(10), 1097–1100.

Robertson, D. J., and D. E. France (1994), Discrimination of remanence-carrying minerals in mixtures, using isothermal remanent magnetisation acquisition curves, *Phys. Earth Planet. Inter.*, *82*, 223–234.
Rochette, P. (1988), La susceptibilite anisotrope des roches faiblement magnétiques: Origines et applications [thèse soutenue sur un ensemble de travaux], Univ. Joseph-Fourier - Grenoble I, Theses.
Schwartz, M., S. P. Lund, D. E. Hammond, R. Schwartz, and K. Wong (1997), Early sediment diagenesis on the Blake/Bahama Outer Ridge, North Atlantic Ocean, and its effects on sediment magnetism, *J. Geophys. Res.*, *102*, 7903–7914, doi:10.1029/96JB03218.
Selkin, P. A., J. S. Gee, L. Tauxe, W. P. Meurer, and A. J. Newell (2000), The effect of remanence anisotropy on paleointensity estimates: A case study from the Archean Stillwater Complex, *Earth Planet. Sci. Lett.*, *183*(3–4), 403–416.
Shcherbakov, V. P., and K. Fabian (2005), On the determination of magnetic grain-size distributions of superparamagnetic particle ensembles using the frequency dependence of susceptibility at different temperatures, *Geophys. J. Int.*, *162*(3), 736–746, doi:10.1111/j.1365-246X.2005.02603.x.
Stephenson, A., S. Sadikun, and D. K. Potter (1986), A theoretical and experimental comparison of the anisotropies of magnetic susceptibility and remanence in rocks and minerals, *Geophys. J. R. Astron. Soc.*, *84*, 185–200.
Stoner, E. C., and E. P. Wohlfarth (1948), A mechanism of magnetic hysteresis in heterogeneous alloys, *Philos. Trans. R. Soc. London, Ser. A*, *240*, 599–642.
Tarduno, J. A. (1995), Superparamagnetism and reduction diagenesis in pelagic sediments: Enhancement or depletion?, *Geophys. Res. Lett.*, *22*, 1337–1340.
Tarling, D. H., and F. Hrouda (1993), *The Magnetic Anisotropy of Rocks*, 1st ed., 217 pp., Chapman and Hall, New York.
Thompson, R., and F. Oldfield (1986), *Environmental Magnetism*, 227 pp., Allen and Unwin, Winchester, Mass.
Worm, H.-U. (1998), On the superparamagnetic–stable single domain transition for magnetite, and frequency dependence of susceptibility, *Geophys. J. Int.*, *133*, 201–206.
Worm, H.-U., and M. Jackson (1988), Theoretical time-temperature relationships of magnetization for distributions of single domain magnetite grains, *Geophys. Res. Lett.*, *15*, 1093–1096.
Worm, H.-U., and M. Jackson (1999), The superparamagnetism of Yucca Mountain Tuff, *J. Geophys. Res.*, *104*(B11), 25,415–25,425.